A metabolomic-based biomarker discovery study for predicting phototherapy duration for neonatal hyperbilirubinemia

Danying Zhu[1,2#], Mingjie Wang[3#], Zhongxiao Zhang[1#], Minghua Liu[3], Yiwen Liu[1], Weiling Wu[3], Dian Lu[3], Xiaoyun Wu[3], Wei Wu[3], Xingyun Wang[1]

[1]Hongqiao International Institute of Medicine, Tongren Hospital, Shanghai Jiao Tong University School of Medicine, Shanghai, China; [2]Department of Respiratory Medicine, Shanghai Children's Hospital, School of Medicine, Shanghai Jiao Tong University, Shanghai, China; [3]Department of Pediatrics, The Second Affiliated Hospital of Nanjing Medical University, Nanjing, China

Contributions: (I) Conception and design: X Wang, W Wu; (II) Administrative support: M Wang; (III) Provision of study materials or patients: M Liu, W Wu; (IV) Collection and assembly of data: D Lu, X Wu; (V) Data analysis and interpretation: D Zhu, Z Zhang, Y Liu; (VI) Manuscript writing: All authors; (VII) Final approval of manuscript: All authors.

[#]These authors contributed equally to this work.

Correspondence to: Xingyun Wang, PhD. Hongqiao International Institute of Medicine, Tongren Hospital, Shanghai Jiao Tong University School of Medicine, No. 720 Xianxia Road, Shanghai 200000, China. Email: wxy@shsmu.edu.cn; Wei Wu, MD. Department of Pediatrics, The Second Affiliated Hospital of Nanjing Medical University, 121 Jiangjiayuan Road, Nanjing 210011, China. Email: wwnj76@sina.com.

Background: Phototherapy is a recommended method for the treatment of neonatal hyperbilirubinemia. However, biomarkers for predicting the more effective duration of phototherapy prior to treatment are lacking. Therefore, we aimed to determine novel predictors for the timing of phototherapy from the perspective of metabolomics.

Methods: A total of 12 newborns with neonatal hyperbilirubinemia were recruited on the day of admission. The infants were divided into a short-duration (<30 hours) phototherapy group and a long-duration (≥30 hours) phototherapy group based on the length of phototherapy treatment. Metabolites in serum samples were then explored using an untargeted metabolomics strategy.

Results: In total, 59 of 1,073 significantly different metabolites were identified between the short-duration and long-duration phototherapy groups, including 18 upregulated and 41 downregulated metabolites. The results of metabolomic analysis showed that the differentially expressed metabolites were enriched in glycerophospholipid metabolism, which is closely associated with the excretion of bilirubin. Moreover, the Kyoto Encyclopedia of Genes and Genomes (KEGG) pathway analysis revealed that the metabolites were also enriched in alpha-Linolenic acid metabolism and fatty acid elongation. Spearman correlation hierarchical clustering analysis demonstrated that 9 metabolites were negatively correlated with the duration of phototherapy. Metabolites, especially phosphatidylethanolamine (PE) (22:1(13Z)/15:0), phosphatidylcholine (PC) (18:1(9Z)/18:1(9Z)), phosphatidylserine (PS) (22:0/15:0), 5,6-dihydrouridine, and PE (MonoMe(11,3)/MonoMe(13,5)), had better predictability for the duration of phototherapy [area under curve (AUC): 1; 95% confidence interval (CI): 1–1] than total serum total bilirubin and direct bilirubin (AUC: 0.806; 95% CI: 0.55–1), as revealed by receiver operating characteristic analysis.

Conclusions: Our research found that the differential metabolites were associated with the duration of neonatal jaundice and that glycerophospholipid metabolism might have played a role in this biological process. Moreover, metabolites such as PE (22:1(13Z)/15:0), PC (18:1(9Z)/18:1(9Z)), PS (22:0/15:0), 5,6-dihydrouridine, and PE (MonoMe(11,3)/MonoMe(13,5)) could be used as predictors for phototherapy duration in neonatal hyperbilirubinemia and assist with decision-making.

Keywords: Neonatal hyperbilirubinemia; metabolites; predict diagnosis; green light; bilirubin encephalopathy

Introduction

Neonatal hyperbilirubinemia, which presents as jaundice, a yellowish discoloration of the skin, sclera, and mucous membranes, affects more than 80% of newborns in the US (1). Severe hyperbilirubinemia will bring about acute bilirubin encephalopathy and kernicterus (2), resulting in long-term neurodevelopmental disabilities or even death (3). One of the mainstay treatments for hyperbilirubinemia is phototherapy, which promotes the formation of water-soluble bilirubin photoisomers that can be excreted through urine and bile (4). Insufficient phototherapy can result in the reappearance of jaundice (5), while excessive treatment commonly leads to fever, diarrhea, and erythematous skin rash, and increase the risk of neoplasm among others (6,7). Current guidance on phototherapy for neonatal hyperbilirubinemia is based on the level of total serum bilirubin (TSB) and the individual risk of neurotoxicity due to excessive bilirubin (8). In addition to the current consensus-based TSB, bilirubin/albumin molar ratio, presence of hemolysis, and the infant's starting TSB, hemoglobin, and rate of bilirubin production will also affect individualized phototherapy (9,10). Thus, it is difficult for doctors to accurately determine the duration of phototherapy in the early stage of hyperbilirubinemia.

Metabolome can provide information on all biochemical activities in a specific biological system at a single time point (11). Diet, pharmacological agents, stress, and other pathological and environmental factors significantly affect the metabolome (11). Subtle variations in metabolism may contribute to identifying the state of the disease. From this, metabolomics studies have been conducted on the diagnosis and prognosis of several diseases, including

pneumonia caused by H1N1 influenza (12), late-onset sepsis in neonates (13), and adverse pregnancy outcomes (14). In addition, metabolomics can be used to further study the molecular mechanisms of infection, immunity, and vaccine response (15). Metabolic disorders themselves may decrease bilirubin clearance in neonatal hyperbilirubinemia, and be regarded as potential biomarkers in the diagnosis of hyperbilirubinemia. Gut metabolites such as gut branched-chain amino acid (including valine, leucine, and isoleucine), proline, methionine, and phenylalanine were elevated in hyperbilirubinemia (16). Serum metabolites including valine, myo-inositol, lysine, leucine, lactate, isoleucine, alanine, creatine, and glycine were increased in neonatal hyperbilirubinemia compared to healthy controls (17).

To discover the distinctive metabolite-based predictors during phototherapy in neonatal hyperbilirubinemia, we used metabolomic analysis to analyze serum metabolites in neonates with hyperbilirubinemia and identified differential metabolites between a short-duration phototherapy group and long-duration phototherapy group. Some of these differential metabolites could be used as predictors of neonatal hyperbilirubinemia in the future. We present the following article in accordance with the MDAR reporting checklist (available at https://tp.amegroups.com/article/view/10.21037/tp-22-637/rc).

Methods

Human samples

A total of 12 hyperbilirubinemia patients who were hospitalized in the neonatology department of the Second Affiliated Hospital of Nanjing Medical University were admitted. All of the patients with low and middle levels of jaundice and did not meet the indication criteria for exchange transfusion based on the guidelines for phototherapy of the American Academy of Pediatrics (18). Except for jaundice, no other clinical manifestations were present in these patients. Blood samples were collected from the peripheral vein on the first day of hospitalization before phototherapy. Informed consent forms were obtained from the parents or their legal guardians. Permission was granted by the ethics committee of the Second Affiliated Hospital of Nanjing Medical University (ethical approval number: [2021]-KY-115-01). The study was conducted in accordance with the Declaration of Helsinki (as revised in 2013). Grouping was done according to the duration of phototherapy: 6 patients with a short duration of

---

Highlight box

Key findings
• The effective biomarkers for predicting duration of phototherapy prior to treatment in neonatal hyperbilirubinemia.

What is known and what is new?
• Current guidance on phototherapy is built on the level of total serum bilirubin.
• Metabolism could be used to analyze serum metabolites and identified differential metabolites between a short-duration and long-duration phototherapy group.

What is the implication, and what should change now?
• Metabolites could be considered as more accurately predictors for phototherapy duration in neonatal hyperbilirubinemia.

---

phototherapy (SDP, less than 30 hours) and 6 patients with a long duration of phototherapy (LDP, 30 hours or more).

Phototherapy

Patients were treated with phototherapy (double-sided LED phototherapy, wavelength ranges from 450–480 nm, the overhead device generated an irradiance of more than 1.7 mW/cm^2, and the underneath device generated an irradiance of more than 0.8 mW/cm^2) and did not receive any other medical interventions. After every 10 hours of continuous phototherapy, patients were treated again at an interval of 4 hours, until at least 2 consecutive TSB measurements returned to normal and showed no increase. The infants were placed in the infant incubator and their eyes and perineum were covered with black cloth. They feed with breast milk and occasional formula supplementation.

Metabolite extraction

Blood samples were separated by centrifugation at 3,000 rpm for 10 minutes. We then transferred 100 µL of each serum sample into a new tube and added 300 µL of methanol solution (containing 5 µg/mL l-2-chlorophenyl alanine) as the internal standard, vortexes for 3 minutes, and centrifuged at 13,000 rpm for 15 minutes at 4 ℃. A total of 100 µL of supernatant was transferred into glass vials for subsequent liquid chromatography–mass spectrometry (LC-MS)/MS. Quality control (QC) samples were prepared by mixing equal volumes of all samples.

LC-MS/MS analysis

For LC-MS/MS analysis, we used the UltiMate 3000 ultra-high performance liquid chromatography (Thermo Fisher Scientific, Waltham, MA, USA) and Orbitrap Elite tandem mass spectrometry (Thermo Fisher Scientific). Chromatographic separation was performed using a Kinetex C18 column (100×2.1 mm, 1.9 µm). The mobile phase consisted of 0.1% formic acid in water (A solution) and 0.1% formic acid in acetonitrile (B solution). The flow rate was 0.4 mL/minute, with the column temperature setting at 25 ℃. The injection volume was 3 µL, with a total run time of 5 minutes. For serum samples, the following gradient setting was applied: 0–2 minutes, 5% B solution; 2–13 minutes, 5–95% B solution; 13–15 minutes, 95% B solution. A 5-minute equilibration step was always applied. Mass spectrometry was carried out in both positive and negative ion modes and the parameters were optimized as follows: for the positive ion mode, heater temperature, 300 ℃; sheath gas flow rate at 45 arb; aux gas flow rate at 15 arb, sweep gas flow rate at 1 arb; spray voltage at 3.0 kV, capillary temperature at 350 ℃, S-lens radio frequency (RF) level at 30%, and the scan range within 50–1,500. For the negative ion mode, heater temperature at 300 ℃, sheath gas flow rate at 45 arb, aux gas flow rate at 15 arb, sweep gas flow rate at 1 arb, spray voltage at 2.5 kV, capillary temperature at 350 ℃, S-lens RF level at 60%, and scan range within 50–1,500.

Statistical analysis

The independent samples *t*-test and Chi-square test were performed with SPSS 23.0, and P<0.05 was considered statistically significant. Compound data was extracted and preprocessed using Compound Discovery 3.0 (Thermo Fisher Scientific), including baseline filtering, retention time correction, peak identification, peak integration, peak alignment, and attribution of the mass spectral fragment. The data was converted into a 2-dimensional data matrix, including the variables (rt m/z, retention time, and mass charge ratio) and normalized peak intensity. SIMCA-P software version 13.0 (Umetrics AB, Umea, Sweden) was used to perform multivariate statistical analysis. Unsupervised principal component analysis (PCA) and supervised partial least squares discriminant analysis (PLS-DA) were performed in both the SDP and LDP groups. The fold changes were visualized using Cytoscape 3.9.1. Pathway evaluations were performed in MetaboAnalyst (http://www.metaboanalyst.ca/) and Kyoto Encyclopedia of Genes and Genomes (KEGG) database (https://www.kegg.jp/). Metabolites were evaluated as biomarkers between SDP and LDP groups using receiver operating characteristic (ROC) analysis. Ingenuity pathway analysis (IPA, http://www.qiagen.com/ingenuity/) was also applied to explore the interaction networks.

Results

Clinical characteristics of the hyperbilirubinemia patients

The average duration of phototherapy was (26.67±5.16) hours in the SDP group and (56.67±10.33) hours in the LDP group. Direct bilirubin (DBIL) levels were markedly lower in the LDP group (272.83±36.02 µmol) compared with the SDP group (318.27±32.27 µmol, P<0.05). There were no significant differences in gestational age, birth

Table 1 Characteristics of infants in the SDP group and LDP group

Baseline information	SDP	LDP	P value
Gestational age (week)	39.38±1.19	38.88±1.04	0.46[a]
Sex (male/female)	4/2	3/3	1.00[b]
Birth weight (kg)	3.54±0.45	3.26±0.46	0.33[a]
Birth mode (natural birth/cesarean section)	3/3	5/1	0.55[b]
Feeding method (breast/formula)	6/0	4/2	0.46[b]
Age on admission (day)	4.83±1.94	3.16±2.03	0.18[a]
TSB (μmol/L)	333.13±34.89	289.28±38.33	0.07[a]
DBIL (μmol/L)	318.27±32.27	272.83±36.02	0.04[a]
Duration of phototherapy (hour)	26.67±5.16	56.67±10.33	<0.01[a]

Values were presented as mean ± SD. [a], Student *t*-test and [b], chi-square test were used for statistical analysis. SDP, short duration of phototherapy; LDP, long duration of phototherapy; TSB, total serum bilirubin; DBIL, direct bilirubin.

weight, age on admission, and TSB between the SDP group and LDP group. Patient information details are shown in *Table 1*.

Multivariate statistical analysis of metabolome

To explore the metabolome differences between the SDP group and LDP group, we performed an LC-MS/MS analysis of serum samples from the patients. PCA showed the distribution of raw data and illustrated that QC samples clustered well (*Figure 1A,1B*). PLS-DA was determined to establish a relationship model between sample categories and metabolite expression. The parameters R^2 and Q^2 were calculated at larger than 0.5 in both positive and negative models, producing good fitness and prediction (*Figure 1C,1D*). Hence, a clear separation of metabolites was observed between the SDP group and the LDP group. To further evaluate the model, a permutation test of PLS-DA was performed. The intercept values of R^2Y (0.0, 0.943) and Q^2 (0.0, –0.0126) showed in the positive mode (*Figure 1E*), and R^2Y (0.0, 0.964) and Q^2 (0.0, –0.021) showed in the negative mode (*Figure 1F*), both implying that our PLS-DA model was not overfitting.

Differential metabolites detected in the SDP and LDP groups

A total of 1,073 metabolites were obtained in the serum samples from the SDP and LDP groups (*Figure 2A*). From both positive and negative ion modes, 59 significantly

differential metabolites (P<0.05) were identified, including 18 upregulated and 41 downregulated ones (*Figure 2B*). The differential metabolites between the 2 groups are listed in *Table 2*.

Pathways analysis of differential metabolites between the SDP and LDP groups

The differential metabolites included 15 identified metabolite categories. Of these, the LDP group contained more steroids and steroid derivatives, carbohydrates and carbohydrate conjugates, other nonmetal organides, and diazines, while purine nucleotides, prenol lipids, organooxygen compounds, heteroaromatic compounds, glycerophospholipids, fatty acyls, ceramides, carboxylic acids and derivatives, and amino acids, peptides, and analogues were higher in the SDP group. Among them, glycerophospholipids showed a significant difference between the 2 groups (*Figure 3A*). To explore the function of the differential metabolites, metabolome pathway analysis using MetaboAnalyst was conducted. The differential metabolites were indicated for their relationship with glycerophospholipid metabolism, glycosylphosphatidylinositol (GPI)-anchor biosynthesis, arginine, and proline metabolism, as well as fatty acid biosynthesis (*Figure 3B*). KEGG pathway analysis also revealed that the metabolites were enriched in glycerophospholipid metabolism, C-type lectin receptor signaling pathway, alpha-linolenic acid metabolism, fatty acid elongation, and linoleic acid metabolism (*Figure 3C*).
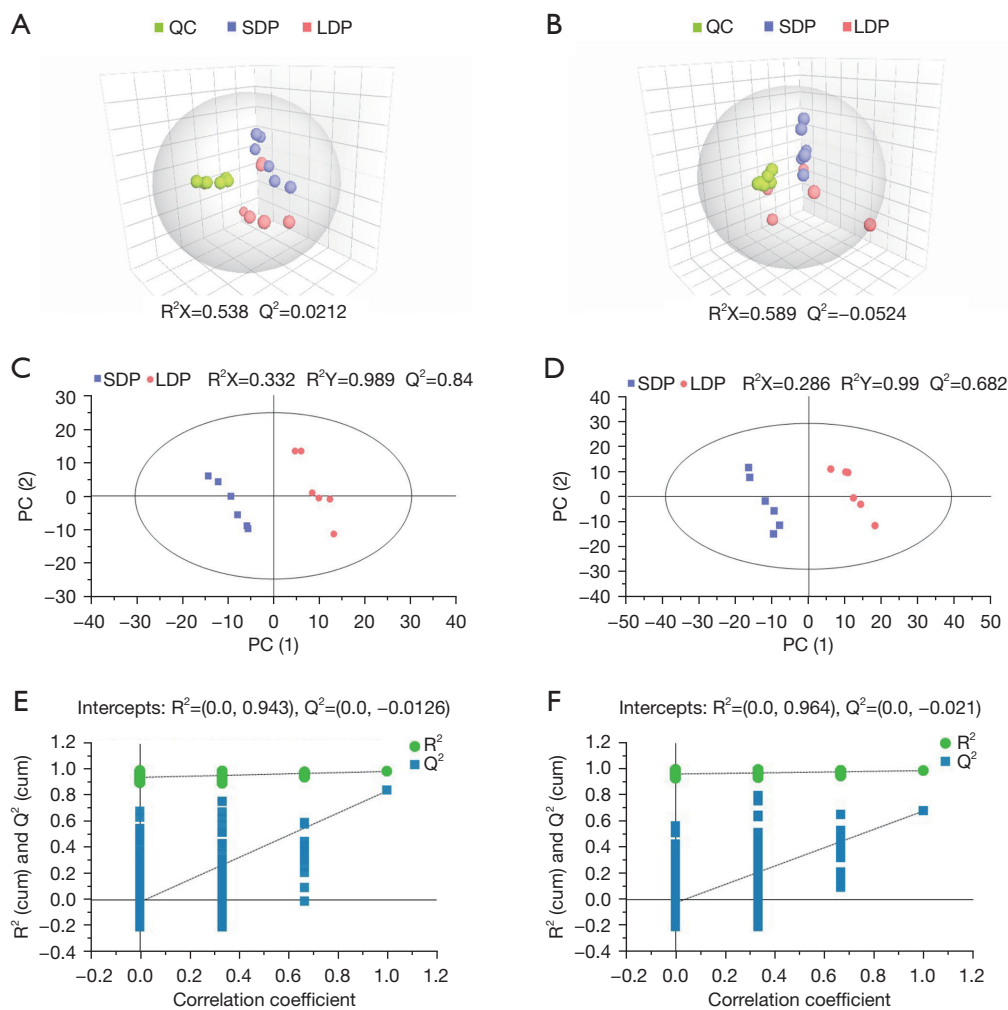
Figure 1 The score plot of the PCA model and the PLS-DA model with a permutation test. (A) Three-dimensional PCA score plot of metabolites in the positive ion mode. (B) Three-dimensional PCA score plot of metabolites in the negative ion mode. The red, purple, and green colors represent the LDP group, SDP group, and QC group, respectively. (C) The PLS-DA score plot of metabolites in the positive ion mode. The x-axis represents the first principal component and the y-axis represents the second principal component. (D) The PLS-DA score plot of metabolites in the negative ion mode. The red and purple colors represent the LDP group and SDP group, respectively. (E) Permutation tests were obtained by the PLS-DA model in the negative ion mode. (F) Permutation tests were obtained by the PLS-DA model in the positive ion mode. QC, quality control; SDP, short duration of phototherapy; LDP, long duration of phototherapy; PCA, principal component analysis; PLS-DA, partial least squares discriminant analysis.

In sum, the glycerophospholipid metabolism pathway was the main pathway involved in the differential metabolites between the 2 groups.

Correlation cluster heat map and association network analysis on the differential metabolites

The correlation between metabolites and clinical characteristics was visualized by hierarchical cluster analysis of Spearman correlation coefficients (*Figure 4A*). Duration of phototherapy had a significant negative correlation with phosphatidic acid (PA) (20:3(5Z,8Z,1Z)/24:0), phosphatidylethanolamine (PE) (MonoMe(11,3)/MonoMe(13,5)), 5,6-dihydrouridine, ubiquinone-9, PE-NMe (22:5(7Z,10Z,13Z,16Z,19Z)/22:4(7Z,10Z,13Z,16Z)), phosphatidylserine (PS) (22:0/15:0), PE (22:1(13Z)/15:0),
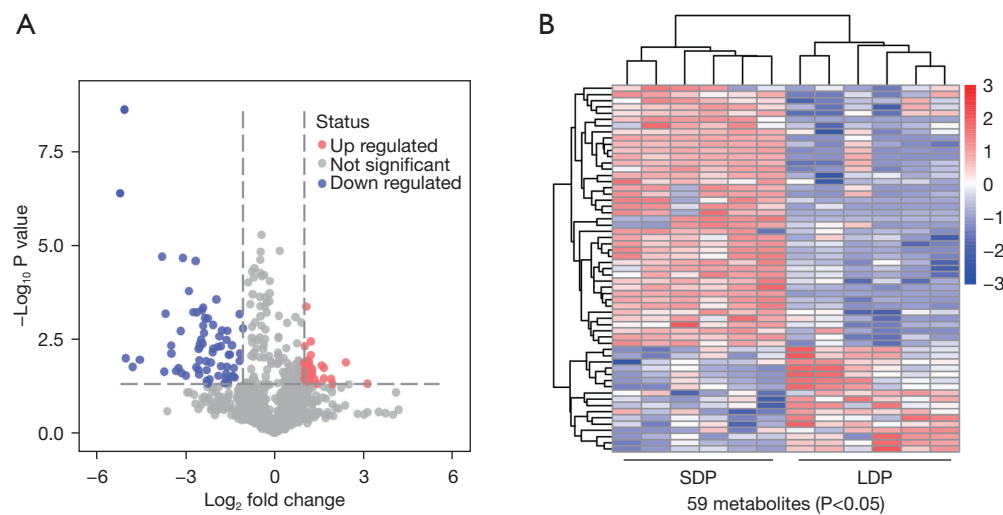
Figure 2 The significantly differential metabolites in the SDP and LDP groups. (A) The volcano plot of the significantly differential metabolites. The significantly downregulated metabolites are indicated by blue dots in the LDP group, the significantly upregulated metabolites are indicated by red dots in the LDP group, and gray dots indicate the metabolites with no significant changes between the 2 groups. (B) The heatmap of hierarchical clustering analysis of the significantly differential metabolites. Increased and decreased metabolite levels are depicted by red and blue colors, respectively. SDP, short duration of phototherapy; LDP, long duration of phototherapy.

phosphatidylcholine (PC) (18:1(9Z)/18:1(9Z)), and propylhexedrine (Spearman correlation coefficient > absolute 0.8). The expressions of the above metabolites were significantly downregulated in the LDP group compared to the SDP group ($P<0.01$) (*Figure 4B*). ROC analysis showed that the model of the above 9 metabolites had better predictive power than TSB and DBIL [area under curve (AUC): 0.806; 95% confidence interval (CI): 0.55–1] (*Figure 5A-5C*). IPA analysis showed that the differentially expressed metabolites might be associated with p38 MAPK and PI3K/Akt signaling pathways (*Figure 6*).

Discussion

Neonatal hyperbilirubinemia is common in newborns and also the main reason for hospitalization in the first week of life (3). Phototherapy is its recommended treatment method and mainly depends on levels of serum TSB (8). The efficacy and duration of phototherapy are affected by various factors, such as TSB, bilirubin/albumin molar ratio, and hemolysis (9), and greater control of phototherapy is needed to reduce toxicity. For clinicians, it is important to accurately identify the method and length of phototherapy treatment in neonatal hyperbilirubinemia and provide accurate medical consultation to parents on the first day of outpatient treatment.

As a consequence, our study focused on identifying distinctive metabolic markers to indicate the duration of phototherapy for neonatal hyperbilirubinemia. Since metabolites participate in modulating the genome, epigenome, transcriptome, and proteome (19), metabolites can act as biomarkers of phenotypic states and also controllers of the phenotype (19). Metabolic derangements could be a cause of decreased bilirubin clearance (20). The unconjugated bilirubin is converted into conjugated bilirubin by uridine 5'-di-glucuronosyltransferase (UDPGT) in the liver (21). Bilirubin is primarily excreted by bile (22), which is composed of cholesterol, bile salts, and bilirubin (23). Most bilirubin is excreted via feces, while a minority is excreted through the kidneys or reabsorbed by the intestine and transported to the liver. Therefore, any disorder of the above process might lead to hyperbilirubinemia. Previous studies demonstrated that phototherapy could accelerate bilirubin metabolism, alter glucose metabolism, and induce lipid peroxidation (17), but have no effect on either oxygen consumption or resting energy expenditure (24). We explored 59 significantly differential metabolites before phototherapy, and most of them were enriched in glycerophospholipids, carboxylic acid and derivatives, as well as organooxygen compounds. The most significant differences were involved in glycerophospholipids, including PA, PC,

Table 2 Significant upregulated and downregulated metabolites between the SDP group and LDP group

Name	HMDB	Molecular weight	RT [min]	P value	Fold change
Upregulated					
Crustecdysone	HMDB0030180	480.30353	7.55	8.28E-04	1.64
LysoPE(18:1(11Z)/0:0)	HMDB0011505	479.30012	7.56	4.17E-03	1.69
Amidosulfonic acid	HMDB34830	96.98337	0.72	8.53E-03	1.09
Palmitic acid	HMDB0000220	256.23991	8.46	1.72E-02	1.42
Cytosine	HMDB0000630	111.0436	10.84	2.00E-02	2.05
Varanic acid	HMDB0002195	436.31822	10.34	2.16E-02	2.24
LysoPA(16:0/0:0)	HMDB0007853	410.2422	8.47	2.17E-02	1.46
LysoPC(18:3(6Z,9Z,12Z)/0:0)	HMDB0010387	517.31315	8.48	2.30E-02	1.38
LysoPC(16:1(9Z)/0:0)	HMDB0010383	493.31647	7.57	2.55E-02	1.74
SM(d18:1/15:0)	HMDB0240608	688.54896	11.29	2.59E-02	2.04
Cholinephosphate	HMDB0001565	183.0658	8.23	2.70E-02	2.17
LysoPC(16:0/0:0)	HMDB0010382	495.33073	8.46	2.71E-02	1.26
LysoPC(20:3(5Z,8Z,11Z)/0:0)	HMDB0010393	545.34695	8.45	3.22E-02	1.44
L-Threose	HMDB0002649	120.0426	0.96	3.49E-02	1.31
Nutriacholic acid	HMDB0000467	390.27631	9.60	3.74E-02	2.54
LysoPC(15:0/0:0)	HMDB0010381	481.3162	7.81	4.01E-02	2.27
LysoPE(0:0/20:1(11Z))	HMDB0011482	507.33229	8.18	4.20E-02	2.14
Downregulated					
N-Acetylglutamine	HMDB0006029	188.07956	1.02	4.43E-04	0.79
Acetyl-L-carnitine	HMDB0240773	204.06059	0.86	5.91E-03	0.77
L-isoglutamine		144.08987	0.95	6.69E-05	0.75
Edetic Acid	HMDB0015109	292.08991	0.98	5.29E-06	0.74
Valylserine	HMDB0029136	204.11091	0.97	1.50E-05	0.73
L-2-Amino-4-methylenepentanedioic acid	HMDB0029433	159.05297	0.97	2.43E-05	0.72
Propylhexedrine	HMDB0015659	155.0482	16.58	9.75E-03	0.71
Threonylglycine	HMDB0029061	176.08003	1.04	2.40E-04	0.71
trans-4-Hydroxy-L-proline	HMDB0000725	131.05801	0.96	3.40E-03	0.68
Mannitol	HMDB0000765	182.07882	0.88	5.69E-03	0.66
2-hexenal	HMDB0031496	98.07298	4.61	4.25E-02	0.64
Glutamylserine	HMDB0028828	234.08514	0.89	1.14E-03	0.64
(4E)-2-Oxohexenoicacid		128.04707	0.88	4.09E-05	0.63
L-Fucose	HMDB0000174	164.06828	0.87	7.39E-03	0.62
5,6-Dihydrouridine	HMDB00497	246.08488	0.96	7.38E-05	0.62
2-Furanmethanol	HMDB0013742	98.03649	0.90	9.39E-03	0.61

Table 2 (*continued*)

Table 2 (*continued*)

Name	HMDB	Molecular weight	RT [min]	P value	Fold change
Alanylthreonine	HMDB0028697	190.09515	0.89	2.03E-04	0.60
dIMP	HMDB0006555	332.04384	0.91	3.88E-03	0.59
L-2,4-Diaminobutyric acid	HMDB06284	216.0743	0.92	5.10E-05	0.59
Ubiquinone-9	HMDB06707	794.62437	16.96	1.68E-03	0.48
PE-NMe2(14:0/20:1(11Z))	HMDB0113859	745.56251	10.25	7.81E-03	0.45
PC(15:0/18:1(11Z))	HMDB0007938	745.56117	7.67	1.24E-02	0.44
9-Oxooctadecanoic acid	HMDB0030979	298.24833	8.83	3.40E-02	0.39
SM(d18:1/18:0)	HMDB0001348	730.59947	11.84	1.89E-02	0.39
PC(22:6(4Z,7Z,10Z,13Z,16Z,19Z)/18:1(9Z))	HMDB0008729	831.57775	16.80	8.43E-03	0.34
PE(MonoMe(11,3)/MonoMe(13,5))	HMDB0061523	851.56518	11.47	1.93E-03	0.33
PE-NMe(20:4(8Z,11Z,14Z,17Z)/22:5 (4Z,7Z,10Z,13Z,16Z))	HMDB0113474	827.54521	12.25	1.77E-02	0.33
PS(18:1(11Z)/15:0)	HMDB0112387	747.5251	10.80	4.77E-02	0.31
PE(22:4(7Z,10Z,13Z,16Z)/P-18:0)	HMDB0009610	779.56477	11.61	1.88E-03	0.29
LacCer(d18:1/12:0)	HMDB0004866	805.55141	8.14	4.93E-03	0.28
PA(20:3(5Z,8Z,11Z)/24:0)	HMDB0115142	810.59672	16.97	2.80E-04	0.26
PE-NMe(22:5(7Z,10Z,13Z,16Z,19Z)/22:4 (7Z,10Z,13Z,16Z))	HMDB0113668	855.59254	9.14	9.01E-04	0.21
PG(i-13:0/a-25:0)	HMDB0116677	806.59981	11.27	2.20E-03	0.19
PS(24:1(15Z)/15:0)	HMDB0112912	831.5959	7.39	5.50E-04	0.18
PS(15:0/24:1(15Z))	HMDB0112341	831.60493	6.56	3.28E-03	0.18
PC(20:5(5Z,8Z,11Z,14Z,17Z)/22:6 (4Z,7Z,10Z,13Z,16Z,19Z))	HMDB0008518	851.5348	10.78	1.19E-02	0.17
PS(22:0/15:0)	HMDB0112709	805.5797	11.57	2.21E-05	0.12
PA(22:0/22:5(4Z,7Z,10Z,13Z,16Z))	HMDB0115170	806.59132	6.56	1.95E-03	0.11
PE-NMe(18:0/22:5(4Z,7Z,10Z,13Z,16Z))	HMDB0113105	807.58778	8.32	6.80E-04	0.08
PS(15:0/22:0)	HMDB0112334	805.59119	6.82	1.77E-02	0.04
PE(22:1(13Z)/15:0)	HMDB0009516	759.57555	11.70	2.47E-09	0.03
PC(18:1(9Z)/18:1(9Z))	HMDB0000593	785.59374	17.00	4.15E-07	0.03

HMDB, the human metabolome database; RT, retention time; SDP, short duration of phototherapy; LDP, long duration of phototherapy; PE, phosphatidylethanolamine; PC, phosphatidylcholine; PS, phosphatidylserine; PA, phosphatidic acid; SM, sphingomyelin; dIMP, deoxyinosine-5'-monophosphate.

PS, phosphatidylglycerol (PG), PE, and corresponding lysophospholipids (25).

Abnormal metabolism of amino acids is also present in neonatal hyperbilirubinemia. As shown in *Table 2*, the LDP group showed increased valylserine, threonylglycine, trans-4-Hydroxy-L-proline, glutamylserine, and alanylthreonine compared with the SDP group. A previous metabolic study by Cai *et al.* found that compared with healthy controls, valine, lysine, leucine, isoleucine, alanine, creatine, and glycine were increased in neonatal jaundice patients, and after phototherapy, metabolites such as valine and pyruvate also changed (17). Another study reported that infants showed a
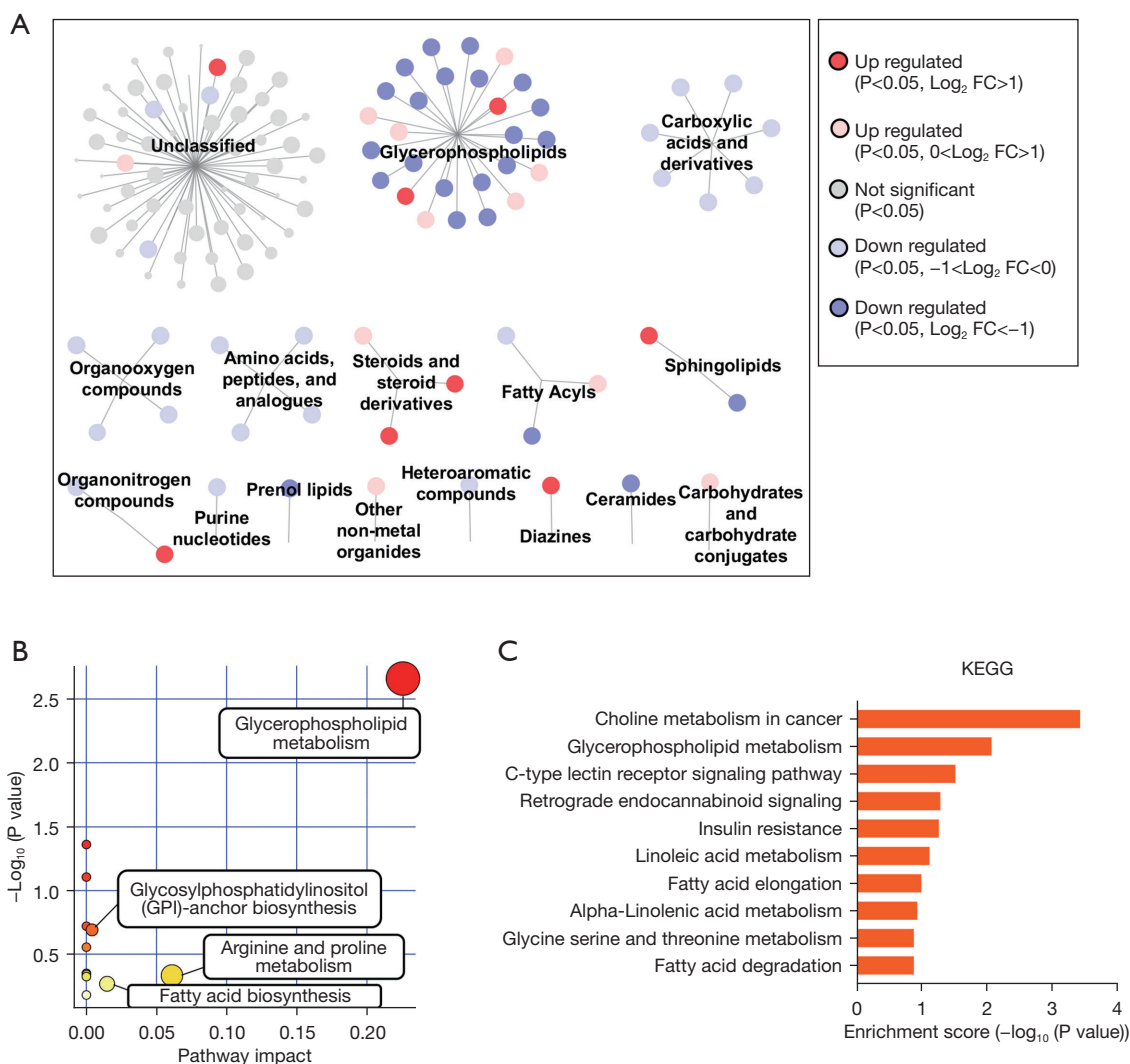
Figure 3 Pathway analysis of significantly differential metabolites. (A) Difference of metabolites among groups visualized by Cytoscape network analysis. The node size is inversely proportional to the magnitude of the P value. Red and blue nodes represent upregulated and downregulated metabolites in the LDP group, respectively. (B) The metabolomic pathway of differential metabolites was analyzed by MetaboAnalyst. The x-axis represents the values computed from the pathway topological analysis, and the y-axis represents the $-\log_{10}$ of the P value. (C) KEGG pathway enrichment analysis of differentially expressed metabolites. FC, fold change; LDP, long duration of phototherapy; KEGG, kyoto encyclopedia of genes and genomes.

higher synthesis rate of albumin when receiving parenteral nutrition with lipids and high-dose amino acids (26). This demonstrated that the levels of those amino acids reduced in the LDP group could lead to the decrease of albumin, which is bound to unconjugated bilirubin and conducive to excretion (27).

To further confirm the relationship between metabolites and the duration of phototherapy, Spearman correlation hierarchical clustering analysis was performed. To directly

examine the prediction of phototherapy, we selected 9 metabolites (Spearman correlation coefficient > absolute 0.8) for ROC analysis, and they all showed a better AUC value than TSB and DBIL. A previous study showed that the solubility of unconjugated bilirubin IXα in bile salt solutions was inhibited by PC, which could compete with the bile salt binding site of IXα (28). Bilirubin could also induce loss of membrane lipids and externalization of PS in human erythrocytes, thus enhancing the production of bilirubin
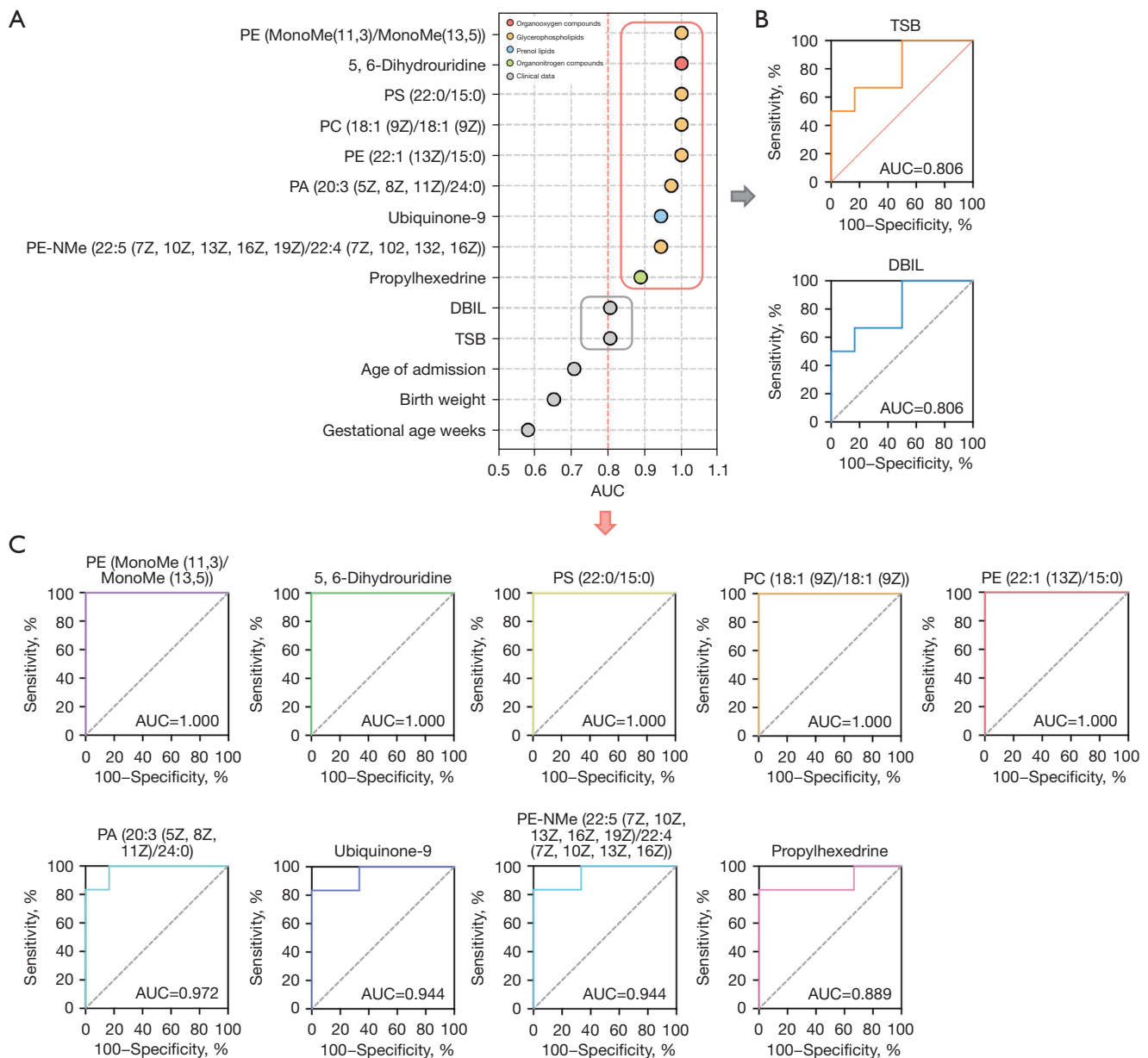
Figure 4 Correlation analysis of metabolites and clinical indicators. (A) Clustering heatmap based on Spearman correlation analysis. The longitudinal direction shows the differential metabolites and the horizontal direction shows the clinical characteristics of patients. The red color indicates a positive correlation and the blue color shows a negative correlation. *, P<0.05; **, P<0.01; ***, P<0.001. (B) The intensity of differential metabolites in the SDP group and LDP group. **, P<0.01. DBIL, direct bilirubin; TSB, total serum bilirubin; SDP, short duration of phototherapy; LDP, long duration of phototherapy; PE, phosphatidylethanolamine; PC, phosphatidylcholine; PS, phosphatidylserine; PA, phosphatidic acid; SM, sphingomyelin.

Figure 5 ROC curves of SDP and LDP groups. (A) ROC of serum metabolic biomarkers and clinical dates to predict the duration of phototherapy in Neonatal hyperbilirubinemia. (B) ROC curves of TSB and DBIL to predict the duration of phototherapy. (C) ROC curves of 9 metabolites to predict the duration of phototherapy. ROC, receiver operating characteristic; AUC, area under ROC curve; DBIL, direct bilirubin; TSB, total serum bilirubin; SDP, short duration of phototherapy; LDP, long duration of phototherapy; PE, phosphatidylethanolamine; PC, phosphatidylcholine; PS, phosphatidylserine; PA, phosphatidic acid.

by facilitating hemolysis and erythrophagocytosis and eventually causing severe neonatal hyperbilirubinemia (29). Cholesterol can be processed into bile acids and participate in steroids (30,31). Ubiquinol is a biomarker of tissue energy requirements and oxidative stress (32), and the subtype ubiquinol-9 is the predominant isoform of a coenzyme that quenches free radicals in the liver (33). Unconjugated bilirubin has been reported as an antioxidant molecule, which could induce apoptosis by activating p38 MAPK (34,35). PI3K/Akt signaling exerts hepatoprotection by promoting
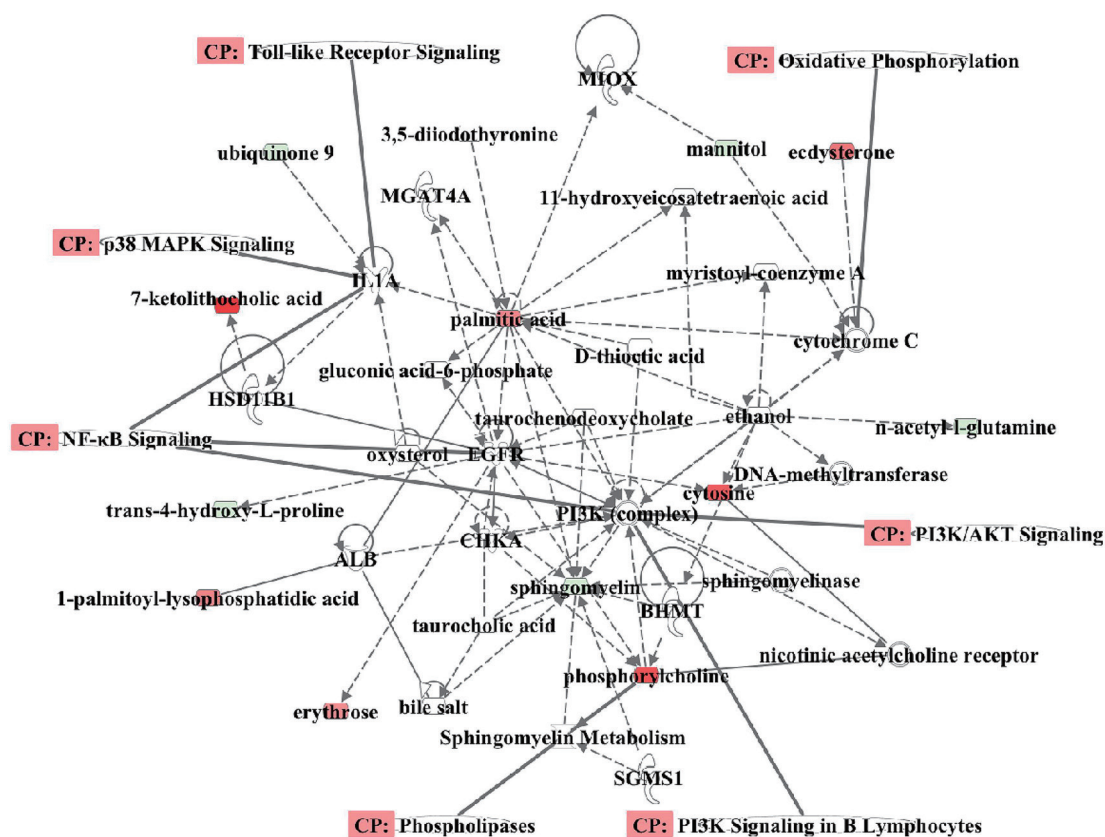
Figure 6 IPA network analysis of the identified differential metabolites. Network enrichment prediction was annotated by IPA software. Green represents downregulated metabolites and red represents upregulated metabolites. IPA, ingenuity pathway analysis; CP, canonical pathways; MAPK, mitogen-activated protein kinase; HSD11B1, hydroxysteroid (11-beta) dehydrogenase 1; NF-κB, nuclear transcription factor-κB; ALB, albumin; CHKA, choline kinase alpha; EGFR, epidermal growth factor receptor; MGAT4A, mannosyl (alpha-1,3-)-glycoprotein beta-1,4-Nacetylglucosaminyltransferase; MIOX, myo-inositol oxygenase, PI3K/AKT, phosphatidylinositol 3 kinase / protein kinase B; BHMT, recombinant betaine homocysteine methyltransferase; SGMS1, sphingomyelin synthase 1.

antioxidant defenses, inactivating reactive oxygen species, and lipid peroxidation (36). These results indicated that oxidation might have played a role in the mechanism of phototherapy. However, our study had some limitations, including the small sample size, and a larger follow-up study is needed to validate our results.

Both biological and environmental factors infect metabolites, and metabolome is thought to be most predictive of phenotype (37). It has been used in the prediction of most diseases and is superior to conventional clinical predictors (38). Localizing metabolic perturbations in patients is also crucial to diagnosing and addressing diseases (39), but species determination is still challenging in metabolomics, the structure and function of numbers of unknown metabolites are waiting for an investigation.

Conclusions

We identified a set of metabolites in neonatal hyperbilirubinemia that could accurately discriminate treatment with a LDP from a short duration. Moreover, metabolites [such as PE (22:1(13Z)/15:0), PC (18:1(9Z)/18:1(9Z)], PS (22:0/15:0), 5,6-dihydrouridine, and PE (MonoMe(11,3)/MonoMe(13,5)) achieved predictability for the length of phototherapy. Our results also suggested that infants with jaundice for a long time had lower levels of glycerophospholipids and increased levels of steroids and steroid derivatives. The differential metabolites participated in various pathways, including p38 MAPK and PI3K/Akt signaling involved in hepatocyte damage caused by bilirubin. Therefore, these metabolites may also

be regarded as potential therapeutic targets in neonatal hyperbilirubinemia.

Footnote

Reporting Checklist: The authors have completed the MDAR reporting checklist. Available at https://tp.amegroups.com/article/view/10.21037/tp-22-637/rc

Data Sharing Statement: Available at https://tp.amegroups.com/article/view/10.21037/tp-22-637/dss

Conflicts of Interest: All authors have completed the ICMJE uniform disclosure form (available at https://tp.amegroups.com/article/view/10.21037/tp-22-637/coif). The authors have no conflicts of interest to declare.

Ethical Statement: The authors are accountable for all aspects of the work in ensuring that questions related to the accuracy or integrity of any part of the work are appropriately investigated and resolved. The written informed consent forms were obtained from the parents or their legal guardians. Permission was granted by the ethics committee of the Second Affiliated Hospital of Nanjing Medical University (ethical approval number: [2021]-KY-115-01). The study was conducted in accordance with the Declaration of Helsinki (as revised in 2013).

References

1. Bhutani VK, Stark AR, Lazzeroni LC, et al. Predischarge screening for severe neonatal hyperbilirubinemia identifies infants who need phototherapy. J Pediatr 2013;162:477-482.e1.

2. Fujiwara R, Haag M, Schaeffeler E, et al. Systemic regulation of bilirubin homeostasis: Potential benefits of hyperbilirubinemia. Hepatology 2018;67:1609-19.

3. Olusanya BO, Kaplan M, Hansen TWR. Neonatal hyperbilirubinaemia: a global perspective. Lancet Child Adolesc Health 2018;2:610-20.

4. Mreihil K, Benth JŠ, Stensvold HJ, et al. Phototherapy is commonly used for neonatal jaundice but greater control is needed to avoid toxicity in the most vulnerable infants. Acta Paediatr 2018;107:611-9.

5. Almohammadi H, Nasef N, Al-Harbi A, et al. Risk Factors and Predictors of Rebound Hyperbilirubinemia in a Term and Late-Preterm Infant with Hemolysis. Am J Perinatol 2022;39:836-43.

6. Joel HN, Mchaile DN, Philemon RN, et al. Effectiveness of FIBEROPTIC phototherapy compared to conventional phototherapy in treating HYPERBILIRUBINEMIA amongst term neonates: a randomized controlled trial. BMC Pediatr 2021;21:32.

7. Bugaiski-Shaked A, Shany E, Mesner O, et al. Association Between Neonatal Phototherapy Exposure and Childhood Neoplasm. J Pediatr 2022;245:111-6.

8. Bhutani VK; Committee on Fetus and Newborn; American Academy of Pediatrics. Phototherapy to prevent severe neonatal hyperbilirubinemia in the newborn infant 35 or more weeks of gestation. Pediatrics 2011;128:e1046-52.

9. Lamola AA. A Pharmacologic View of Phototherapy. Clin Perinatol 2016;43:259-76.

10. Donneborg ML, Vandborg PK, Hansen BM, et al. The impact of hemoglobin on the efficacy of phototherapy in hyperbilirubinemic infants. Pediatr Res 2017;82:947-51.

11. Bahado-Singh RO, Ertl R, Mandal R, et al. Metabolomic prediction of fetal congenital heart defect in the first trimester. Am J Obstet Gynecol 2014;211:240.e1-240.e14.

12. Banoei MM, Vogel HJ, Weljie AM, et al. Plasma metabolomics for the diagnosis and prognosis of H1N1 influenza pneumonia. Crit Care 2017;21:97.

13. Sarafidis K, Chatziioannou AC, Thomaidou A, et al. Urine metabolomics in neonates with late-onset sepsis in a case-control study. Sci Rep 2017;7:45506.

14. Lee SM, Lee EM, Park JK, et al. Metabolic Biomarkers In Midtrimester Maternal Plasma Can Accurately Predict Adverse Pregnancy Outcome in Patients with SLE. Sci

Rep 2019;9:15169.

15. Diray-Arce J, Conti MG, Petrova B, et al. Integrative Metabolomics to Identify Molecular Signatures of Responses to Vaccines and Infections. Metabolites 2020;10:492.

16. Zeng S, Wang Z, Zhang P, et al. Machine learning approach identifies meconium metabolites as potential biomarkers of neonatal hyperbilirubinemia. Comput Struct Biotechnol J 2022;20:1778-84.

17. Cai A, Qi S, Su Z, et al. A Pilot Metabolic Profiling Study of Patients With Neonatal Jaundice and Response to Phototherapy. Clin Transl Sci 2016;9:216-20.

18. American Academy of Pediatrics Subcommittee on Hyperbilirubinemia. Management of hyperbilirubinemia in the newborn infant 35 or more weeks of gestation. Pediatrics 2004;114:297-316.

19. Rinschen MM, Ivanisevic J, Giera M, et al. Identification of bioactive metabolites using activity metabolomics. Nat Rev Mol Cell Biol 2019;20:353-67.

20. Schwartz HP, Haberman BE, Ruddy RM. Hyperbilirubinemia: current guidelines and emerging therapies. Pediatr Emerg Care 2011;27:884-9.

21. Moschos SJ, Sullivan RJ, Hwu WJ, et al. Development of MK-8353, an orally administered ERK1/2 inhibitor, in patients with advanced solid tumors. JCI Insight 2018;3:e92352.

22. Meixiong J, Vasavda C, Green D, et al. Identification of a bilirubin receptor that may mediate a component of cholestatic itch. Elife 2019;8:e44116.

23. Kelly SM, Lanigan N, O'Neill IJ, et al. Bifidobacterial biofilm formation is a multifactorial adaptive phenomenon in response to bile exposure. Sci Rep 2020;10:11598.

24. Fok TF, Gu JS, Lim CN, et al. Oxygen consumption and resting energy expenditure during phototherapy in full term and preterm newborn infants. Arch Dis Child Fetal Neonatal Ed 2001;85:F49-52.

25. Zhou C, He M, Peng C, et al. Pharmacokinetic and Lipidomic Assessment of the In Vivo Effects of Parishin A-Isorhynchophylline in Rat Migraine Models. J Anal Methods Chem 2020;2020:9101598.

26. Vlaardingerbroek H, Schierbeek H, Rook D, et al. Albumin synthesis in very low birth weight infants is enhanced by early parenteral lipid and high-dose amino acid administration. Clin Nutr 2016;35:344-50.

27. Neonatal jaundice: Evidence Update March 2012. London: National Institute for Health and Care Excellence (NICE); 2012.

28. Berman MD, Carey MC. Metastable and equilibrium phase diagrams of unconjugated bilirubin IXα as functions of pH in model bile systems: Implications for pigment gallstone formation. Am J Physiol Gastrointest Liver Physiol 2015;308:G42-55.

29. Brito MA, Silva RF, Brites D. Bilirubin induces loss of membrane lipids and exposure of phosphatidylserine in human erythrocytes. Cell Biol Toxicol 2002;18:181-92.

30. Buitenwerf E, Dullaart RPF, Muller Kobold AC, et al. Cholesterol delivery to the adrenal glands estimated by adrenal venous sampling: An in vivo model to determine the contribution of circulating lipoproteins to steroidogenesis in humans. J Clin Lipidol 2017;11:733-8.

31. Clos-Garcia M, Garcia K, Alonso C, et al. Integrative Analysis of Fecal Metagenomics and Metabolomics in Colorectal Cancer. Cancers (Basel) 2020;12:1142.

32. Miles L, Miles MV, Tang PH, et al. Ubiquinol: a potential biomarker for tissue energy requirements and oxidative stress. Clin Chim Acta 2005;360:87-96.

33. Khan SA. Effects of dehydroepiandrosterone (DHEA) on ubiquinone and catalase in the livers of male F-344 rats. Biol Pharm Bull 2005;28:1301-3.

34. Tell G, Gustincich S. Redox state, oxidative stress, and molecular mechanisms of protective and toxic effects of bilirubin on cells. Curr Pharm Des 2009;15:2908-14.

35. Khan NM, Poduval TB. Immunomodulatory and immunotoxic effects of bilirubin: molecular mechanisms. J Leukoc Biol 2011;90:997-1015.

36. Xu Y, Jiang Y, Li Y. Pyrazinamide enhances lipid peroxidation and antioxidant levels to induce liver injury in rat models through PI3k/Akt inhibition. Toxicol Res (Camb) 2020;9:149-57.

37. Schrimpe-Rutledge AC, Codreanu SG, Sherrod SD, et al. Untargeted Metabolomics Strategies-Challenges and Emerging Directions. J Am Soc Mass Spectrom 2016;27:1897-905.

38. Buergel T, Steinfeldt J, Ruyoga G, et al. Metabolomic profiles predict individual multidisease outcomes. Nat Med 2022;28:2309-20.

39. DeBerardinis RJ, Keshari KR. Metabolic analysis as a driver for discovery, diagnosis, and therapy. Cell 2022;185:2678-89.